Since January 2020 Elsevier has created a COVID-19 resource centre with free information in English and Mandarin on the novel coronavirus COVID-19. The COVID-19 resource centre is hosted on Elsevier Connect, the company's public news and information website.

Informatics in Medicine Unlocked 32 (2022) 101025

Contents lists available at ScienceDirect

Informatics in Medicine Unlocked

journal homepage: www.elsevier.com/locate/imu

Artificial intelligence enabled non-invasive T-ray imaging technique for early detection of coronavirus infected patients

Swarnava Biswas [a,1], Saikat Adhikari [b,1], Riddhi Chawla [c], Niladri Maiti [c], Dinesh Bhatia [d], Pranjal Phukan [e], Moumita Mukherjee [b,*]

[a] School of Health Sciences, The Neotia University, Kolkata, West Bengal, India
[b] Department of Physics, School of Basic & Applied Sciences, Adamas University, Kolkata, West Bengal, India
[c] Medical School, Akfa University, Tashkent, Uzbekistan
[d] Department of Biomedical Engineering, North Eastern Hill University, Shillong, Meghalaya, India
[e] Department of Radiology and Imaging, North Eastern Indira Gandhi Regional Institute of Health and Medical Sciences, Shillong, Meghalaya, India

ARTICLE INFO

Keywords:
Avalanche transit time device
Coronavirus disease
Large-signal impedance and admittance study
Non-linear quantum drift-diffusion simulator
Room temperature characteristics
Terahertz source and radiation system
T-ray thermograph study

ABSTRACT

A new artificial intelligence (AI) supported T-Ray imaging system designed and implemented for non-invasive and non-ionizing screening for coronavirus-affected patients. The new system has the potential to replace the standard conventional X-Ray based imaging modality of virus detection. This research article reports the development of solid state room temperature terahertz source for thermograph study. Exposure time and radiation energy are optimized through several real-time experiments. During its incubation period, Coronavirus stays within the cell of the upper respiratory tract and its presence often causes an increased level of blood supply to the virus-affected cells/inter-cellular region that results in a localized increase of water content in those cells & tissues in comparison to its neighbouring normal cells. Under THz-radiation exposure, the incident energy gets absorbed more in virus-affected cells/inter-cellular region and gets heated; thus, the sharp temperature gradient is observed in the corresponding thermograph study. Additionally, structural changes in virus-affected zones make a significant contribution in getting better contrast in thermographs. Considering the effectiveness of the Artificial Intelligence (AI) analysis tool in various medical diagnoses, the authors have employed an explainable AI-assisted methodology to correctly identify and mark the affected pulmonary region for the developed imaging technique and thus validate the model. This AI-enabled non-ionizing THz-thermography method is expected to address the voids in early COVID diagnosis, at the onset of infection.

1. Introduction

The novel Coronavirus pandemic [1] began in Wuhan, a province of the People's Republic of China, with an onset of an unknown severe respiratory ailment (pneumonia) [2]. The pathogen of the sickness was identified as a novel coronavirus and given the name SARS-CoV-2 (Severe Acute Respiratory Syndrome Coronavirus 2) [3] and the disease was given the name COVID-19 (Corona Virus Disease) [4]. The virus is highly contagious and can transmit from person to person within six feet of an infected individual via respiratory droplets [5]. The virus is transmitted via the respiratory tract. Coronavirus enters the body and begins infecting the epithelial cells of the respiratory tract [6] and gradually begins penetrating the host cell [7]. Inside the host cells, the virus initiates replication and continues to multiply until the cell dies. Coronavirus replication continues, and as it progresses down the windpipe and into the lungs, it causes more serious respiratory disorders such as bronchitis and pneumonia [7]. RTPCR (Reverse Transcription – Polymerase Chain)/Nucleic Acid testing and radiographic imaging are

Abbreviations: AI- Artificial Intelligence, COVID- Corona Virus Disease; SARS-CoV-2- Severe Acute Respiratory Syndrome Coronavirus 2, THz- Terahertz; Tray- Terahertz Ray, CT Scan- Computed Tomography Scan; FEM-finite element method, CNN- Convolution Neural Network; ATT- Avalanche Transit Time, SNR-signal-to-noise ratio; RCNN- Region-Based Convolutional Neural Network, RPN- Region Proposal Network; RoI- Regions of Interest, FBP- Full Body Prosthetics; ConvNet- Convolutional Network, aLaRa- as Low as Reasonably achievable.

* Corresponding author.
E-mail addresses: moumita.mukherjee@adamasuniversity.ac.in, drmmukherjee07@gmail.com (M. Mukherjee).
[1] Equal Contribution.

https://doi.org/10.1016/j.imu.2022.101025
Received 20 June 2022; Received in revised form 12 July 2022; Accepted 15 July 2022
Available online 20 July 2022

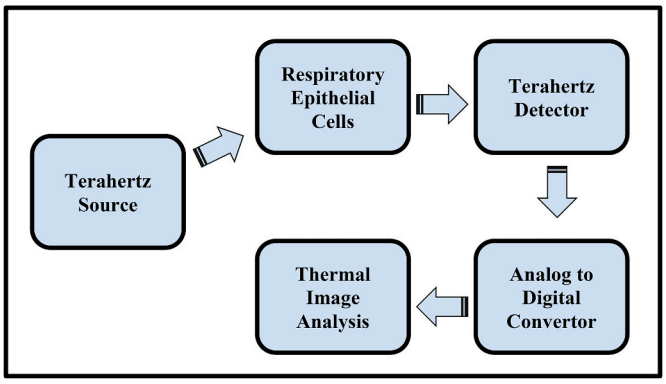

Fig. 1. Block Diagram of THz-thermal imaging system for coronavirus screening purpose.

existing diagnosing and screening modalities for coronavirus infected patients. Recently Rapid Antigen Tests are also considered for at-home COVID detection. However, they suffer severely with false-positive and false-negative results. Imaging modalities are X-Ray [8–10] based and as a result, frequent application for screening and monitoring purposes is not recommended [11]. Early diagnosis of the disease using CT scan investigation has suffered from serious limitations, because of the fact that more than fifty percent of new sufferers in China have shown healthy CT scan reports during the early stage of the disease [12,13]. On the other hand, in this research article, the authors have proposed a non-invasive method, for the early stage detection of coronavirus infected patients, using non-ionizing terahertz radiation source for imaging purposes. Owing to its non-ionizing characteristics, the T-Ray imaging technique can be used safely for coronavirus screening and monitoring purposes. Moreover, AI-enabled T-Ray imaging technique will definitely enhance the efficacy of disease detection at the very onset and thus the infection can be arrested before spreading into the lower respiratory tract. In this way, the proposed technique can be suitably used for saving lives.

Here they have developed a room temperature terahertz source for the study and reported elsewhere [14–18]. The radiation coming out from the waveguide embedded THz-solid-state source is incident on the human respiratory tract and THz thermographs are generated and an image analyzer is placed for analyzing the output. The finite element method (FEM) is adopted and studied in COMSOL Multiphysics (5.3a) software for Terahertz frequencies [19,20]. The analysis is based on the identification of the optimum transmission direction at the interface layers from an external Terahertz source. The study reveals that ~100 GHz (0.1 THz) incident radiation power would be ideal for this application. The proposed THz-thermal scanning workflow diagram is described in Fig. 1. Earlier, THz spectroscopy was used for the study of protein, glucose, yeast, and also for viruses [21]. Recently Terahertz (0.1 THz – 10 THz) imaging and spectroscopy technology have been immersed as effective methods to study biomolecules [22–24]. Compared to X-Ray radiation (used for CT scan), THz-radiation is completely safe for biomedical uses [25–27]. THz-signal provides a good balance between spatial resolution and depth of penetration for biomedical applications [28,29]. When the human body is exposed to the coronavirus and becomes infected, uncontrolled cell proliferation occurs [30]. Virus affected zone would have a significantly higher water content than normal cells/tissues. As a result of the varying electrical/dielectric/thermal characteristics of respiratory epithelium cells, the radiation power absorption is significantly higher in the abnormal/affected areas. These finally result in an elevated cell temperature in the affected portion compared to healthy neighbouring cells and thus produce a sharp temperature gradient on thermographs.

Using the aforementioned imaging approach, an AI-assisted image analyzer was created to evaluate THz thermographs. The class returned as output has strong visualisation capability. By integrating Convolution Neural Network's (CNN) accurate prediction and explainable feature through network visualisation, a flexible end-to-end detection approach is suggested [31]. This mimics a doctor's approach while revealing imaging constraints. Deep networks are meant to perform things humans can easily do, therefore they've been used in medical diagnosis for some time. These models use tagged datasets and multi-layered neural network architectures. The network learns shallow to detailed characteristics directly from the data using a cascaded structure of convolutional modules. Convolutional modules use a set number of 2-D convolutional filters, making them effective for image processing. In this research, the authors present a model architecture in which the CNN classifies Terahertz thermographs into COVID and NON-COVID subjects. The study is the first to analyze coronavirus patients using AI-enabled THz-thermographs.

2. Model description

2.1. In-silico thermal imaging study

A solid-state room temperature terahertz source is developed using standard microelectronics fabrication process steps [32]. The details of the design and the development of the source are reported elsewhere [14–18]. The position of the source with respect to the detector is varied for getting the optimum penetration depth. The radiation energy and exposure time are adjusted in such a way that the electromagnetic radiation energy safety protocol is maintained. Radiation safety protocol are mostly applicable for ionizing radiation like X-ray based diagnostic systems. Terahertz is non ionizing radiation. Three basic principles should be adhered to when dealing with radiation and making radiographs: Time, Distance and Shielding. These principles form the basis of a broader radiation safety concept called aLaRa (as Low as Reasonably achievable). For terahertz imaging, the authors have taken care of dose, energy distance and time of exposure. The cell temperature should not increase beyond 46 °C, beyond this cell damage happens.

In the present model the author has taken care of this. The distance of exposure, energy and time of exposure are optimized through several computer run. Although T-ray is promising for various biomedical applications, the in-vivo penetration depth adjustment is a challenge in real-time experiments. This is because the absorption of T-ray energy within the body water cell is so significant, that an appreciable amount of energy gets absorbed and negligible energy is penetrated carrying the information of the virus-affected zone. The authors have incorporated the photon-coupling method in the system to enhance the penetration depth through the human body organ by adjusting the signal-to-noise ratio (SNR).

In this paper, the authors have used a vertically doped Avalanche Transit Time (ATT) oscillator. Due to the limitation of the application of terahertz energy straightway in the human body, the authors have

Table 1
Cell properties considered for thermograph generation model in COMSOL Multiphysics (5.3a).

Cell/Tissue	Electrical conductivity (S/m)	Thermal Conductivity (W/mK)	Relative permittivity	Density (Kg/m^3)	Specific Heat capacity (J/Kg K)
Respiratory epithelium cell (healthy)	2.50	0.302	20.50	260.0	2560.0
Respiratory epithelium cell (virus affected)	3.0	0.310	23.0	350.0	2560.0

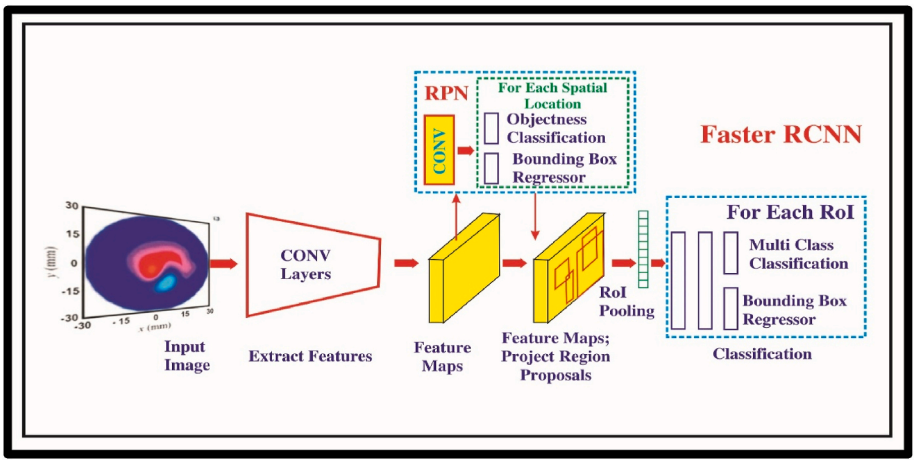

Fig. 2. Typical steps of faster Region-Based Convolutional Neural Network.

developed a phantom model of upper respiratory systems through COMSOL Multiphysics (5.3a) software and simulated the models. In the COMSOL Multiphysics (5.3a) study, the problem domain consists of a respiratory organ, virus affected and healthy surrounding cells, and a THz-radiation source (radiating antenna). The organ under test is assumed to be 75 mm × 30 mm in dimension. The distance between the source and the sample is optimized to 10 cm for getting the best result. The bio-heat transfer model is adopted for the present study. The design parameters are given in Table 1. COMSOL Multiphysics (5.3a) simulator solves the 3D-heat conduction equation using the finite element method. THz thermographs are generated by: (a) moving the specimen for a fixed radiation source and detector (b) by moving the radiation source and detector keeping the sample under test at a fixed position. In this work, the authors have chosen option (b). The absolute thermal contrast is the variable adopted to analyze the dielectric variation in cells:

$$\Delta T\,(x,y,t) = T_d\,(x,y,t) - T_S\,(x,y,t) \tag{1}$$

Where T_d denotes the pixel temperature of the affected zone and T_S corresponds to the non-affected zone. Input power and initial cell temperature (before exposure) are considered as 10W and 37 °C, respectively.

Maxwell's equations are solved subject to appropriate boundary conditions. The calculation is carried out to determine the specific electromagnetic absorption rate (SAR). The following is the solution of the bioheat equation [33] in order to generate a respiratory tract thermograph model that includes both cells/tissues that are healthy and diseased. An axisymmetric magnetic transversal formulation is used for the development of an *in-silico* biological model. Following that, the Maxwell Equations [33] are simplified to a wave equation in:

$$\nabla x\left[\left(\varepsilon_r - \frac{j\sigma_E}{\omega\varepsilon_0}\right)^{-1}\nabla x\vec{H_\varphi}\right] - \mu_r k_0^2 \vec{H_\varphi} = 0 \tag{2}$$

Where electrical conductivity is represented by σ_E. From Eq. (2), the magnetic field $\vec{H}$ is solved and then the simulation is done with electric field $\vec{E}$. Let unit normal vector for a surface as $\vec{n}$ is,

$$\vec{n} x \vec{E} = 0 \tag{3}$$

The first-order boundary condition [33] is used at outer boundaries of cells:

$$\vec{n} x\sqrt{\bar{\varepsilon}}\vec{E} - \sqrt{\bar{\mu}}\vec{H_\varnothing} = -2\sqrt{\bar{\mu}}\vec{H_{\varnothing 0}} \tag{4}$$

Details of the terahertz generation methodology, as developed by the authors, is given elsewhere [28]. Blood perfusion, dielectric and thermal characteristics of infected and normal tissues are complex functions of the EM waves and frequency of oscillation [34]. The corresponding

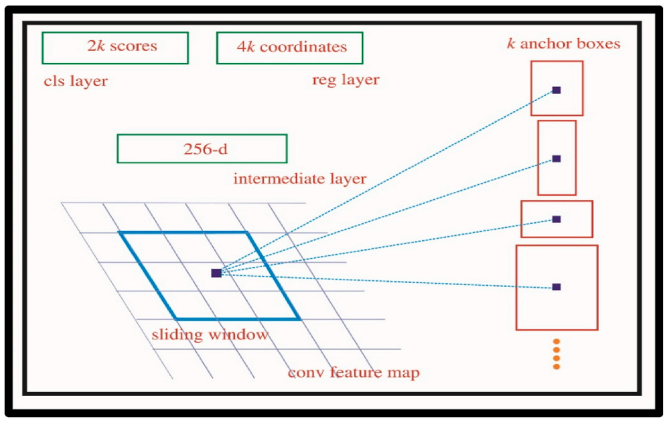

Fig. 3. Workflow diagram of faster Region-Based Convolutional Neural Network.

experimentally verified cellular properties are summarized in Table 1 [33,35,36].

The Convolution Neural Network (CNN) has long been a tool of choice for processing and analyzing images. The Region-Based Convolutional Neural Networks (R–CNN) model to identify infected and normal terahertz has been trained with the processed images [37]. Detectron2, a Faster–RCNN algorithm, is applied in this case. Faster-RCNN is a fork of the Fast-RCNN algorithm [38]. The primary distinction between them is that Fast-RCNN generates Regions of Interest (RoI) using selective search, whereas Faster RCNN utilizes a "Region Proposal Network," or RPN. RPN accepts picture feature maps as input and provides output as a series of object proposals, each with a score for object-ness [39]. In a Faster-RCNN technique, the following stages are commonly followed as described in Fig. 2:

1. Bypassing an image as input to the ConvNet, which returns the feature map.
2. These feature maps are subjected to an RPN. This method returns the object proposals together with a score indicating their object-ness.
3. Based on these ideas, a RoI for the pooling layer is performed to reduce their size to the same level.
4. Finally, the proposals are given to a fully connected layer with linear regression and softmax on top, which classifies and provides the output.

To begin, Faster-RCNN transfers CNN's feature maps to the RPN, which creates k anchor boxes of varying shapes and sizes by sliding a

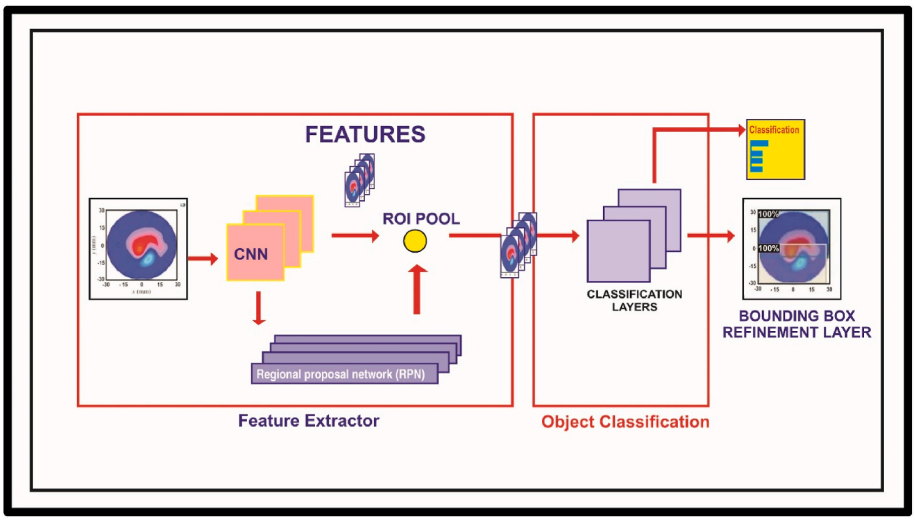

Fig. 4. Generation of feature maps from T-Ray thermographs with required dimension details.

window over all these feature maps. The workflow is described in Fig. 3.

Anchor boxes are fixed-size boundary boxes that are positioned randomly across the image and come in a variety of shapes and sizes; the details are provided elsewhere [40]. It generates feature maps of defined dimensions for each anchor and it is described in Fig. 4.

The feature maps are then sent to a fully connected layer equipped with a softmax and a linear regression layer [41]. Finally, it classifies the item and forecasts its bounding boxes.

The day to day progression of the disease has been captured by Terahertz based imaging and the same has been used as an input feed to the network. Needless to mention that the algorithm is supervised classifiers hence the captured images must be fed with their corresponding labels. The distribution of data set into Training and Testing is as follows, total images = 400, training set = 320 and test set = 80.

3. Results and discussion

T-Ray is invisible to the eye like X-rays and Gamma-Ray & sandwiched in the gap between microwaves and Infrared light waves. This part of the electromagnetic spectrum is called the "Terahertz Gap" because of the unavailability of suitable sources for its useful applications. Terahertz radiations have certain important properties: its non-ionizing nature doesn't put so much energy into the object that it starts to change its composition. This is the major advantage over X-Rays, i.e. more powerful but ionizing, and thus X-Ray has the potential to disrupt the molecular bond of the living tissues. T-Ray operates in pulse modes like radar and ultrasound, thus we can get information about the range and depth of the object. Recently, a super lattice terahertz device for precise cancer cell detection in a full-body prosthetic (FBP) has been constructed and investigated by Adhikari et. Al [42,43]. Thermographic detection of malignant tumours in Full Body Prosthetics (FBP) is reported here, and the authors present a large-signal model of a THz Solid State Imaging System for this purpose. Biswas et. Al in their publication, presented a novel method of diagnosing Alzheimer's disease (AD) by using THz thermograms [44]. This research proposed a room-temperature, solid-state generator of THz radiation and it uses an in-house designed quantum modified classical drift diffusion simulator to investigate the THz non-linear characteristics of the device and system. Adhikari et al. also proposed a solid state device that can work at room temperature for the non-invasive detection of hepatic cell carcinoma [45]. Again Adhikari et al. in their study, described the development of an in-silico T-ray thermal imaging and detection system for the diagnosis and early detection of breast cancer [46]. From all the studies it is clear that, the healthy epithelium cells damage due to microwave or any other ionizing radiations and THz exposure under similar operating conditions are different. THz is found to be safer than microwave radiation or X-Ray as far as percentage of neighbouring cell damage is concerned.

At the outset of the assessment, numerous grid resolutions are evaluated and compared to find the most suitable one to ensure the highest accuracy. For terahertz wave frequency, 0.1 THz, the default grids and refined grids are shown in Fig. 5.

Healthy respiratory epithelium cells are considered for study under the Terahertz (0.1 THz) exposure for 10 s. The time of exposure and

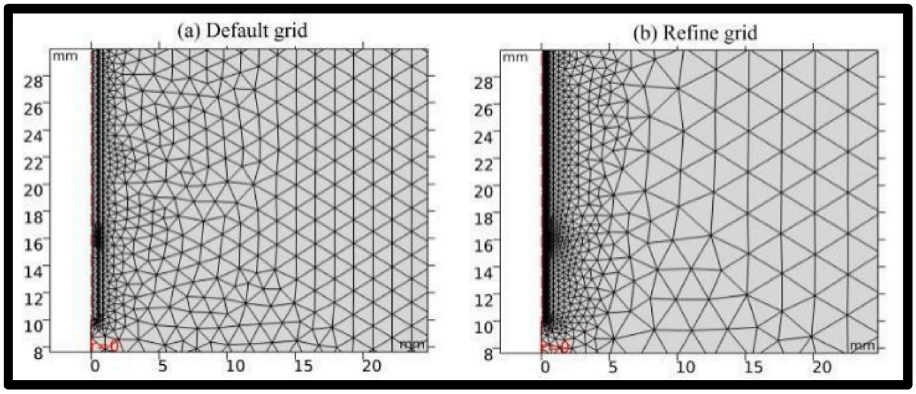

Fig. 5. Grid design for thermograph study under Terahertz exposure (Comsol multiphysics 5.3 a).

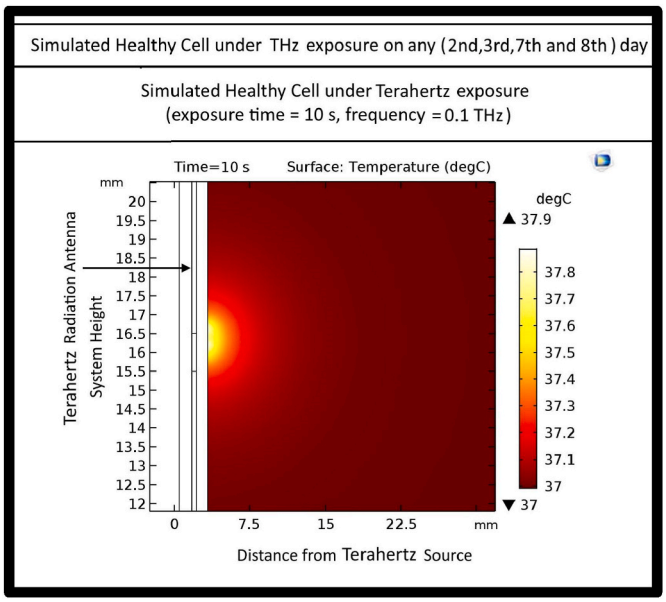

Fig. 6. THz thermographs for simulated healthy respiratory cells on 2nd, 3rd, 7th and 8th day of infection.

incident power is optimized through the experiment, considering the cell burnout issues due to excessive heat generation. Fig. 6 denotes the effect of terahertz exposure on healthy cells tested on the second, third, seventh, and eighth day of the experiment. The thermographs are not showing any significant temperature gradient after 10 s of exposure. This is because all healthy cells will absorb the incident energy uniformly and thus the question of red spot/hotspot doesn't arise.

Fig. 7(a–d) depicts the effect of terahertz exposure on virus-affected respiratory epithelium cells mixed with healthy cells. This is interesting to observe that virus-affected cells have absorbed more terahertz energy/radiation power than healthy cells and thus there is a slight indicative temperature gradient in comparison to Fig. 6. Moreover, this temperature gradient is slightly more prominent under THz exposure.

Fig. 7(b) denotes the THz thermographs obtained on the third day of infection. With the advancement of the day, the spreading of infection increases, and this is reflected in Fig. 7(c and d). On the 7th and 8th day of infection, the spreading in the neighbouring epithelial cells is significant and thus the temperature gradient arises due to non-uniform power absorption in healthy and non-healthy epithelial cells, is significantly high under THz exposure. The significant temperature gradient on the 8th day of infection is a sure indication of the presence of unhealthy/infected cells that can be utilized for viral infection screening.

Fig. 8 shows the circular cross-sectional view of the sample under test subject to THz radiation for 10 s. The THz radiation thermography can detect the (x, y) position and degree of viral infection effectively. The temperature gradient is much more prominent in THz thermography during the 2nd to 8th day of infection. Thus, early detection of COVID infection is possible with THz thermography and the same can be used as a basic screening tool in COVID-affected patients.

Thus, a reliable screening technique will play an important role to stop community spreading. Terahertz radiation is non-ionizing in nature can be used safely for thermal imaging of upper respiratory track unrestrictedly. When the virus-affected patient is asymptomatic, T-Ray imaging of the upper respiratory tract will show thermal hotspots that signify the existence of viral infection in the very early stage. With the spreading of the infection, the location of the hotspot will spread and the day-to-day monitoring of the disease would be possible. This will also help to isolate the suspected person from the mass gathering and thus contact spreading can be avoided largely. In this way, the T-Ray imaging

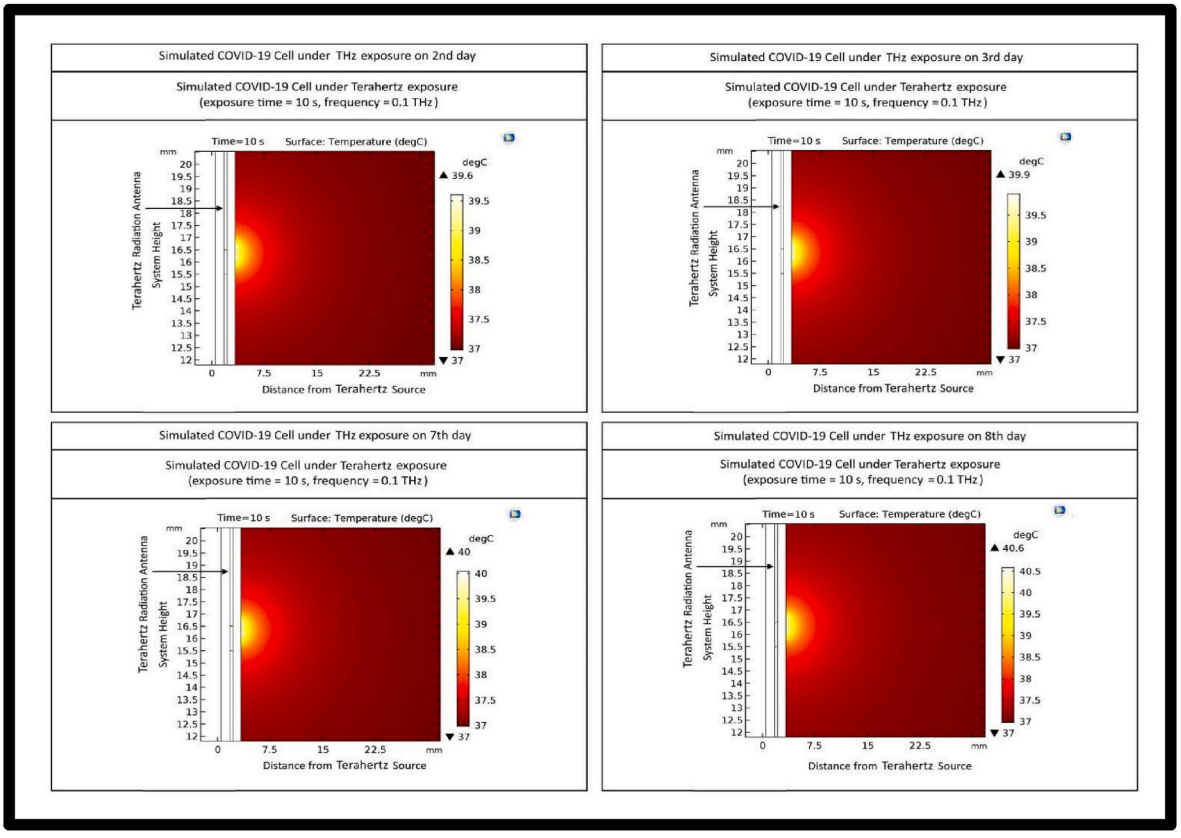

Fig. 7. THz thermographs of nCOVID-19 affected respiratory cell on (a) 2nd day (b) 3rd (c) 7th day and (d) 8th day dayof virus exposure (within incubation period): optimized exposure time = 10 s (Comsol multiphysics 5.3 a).

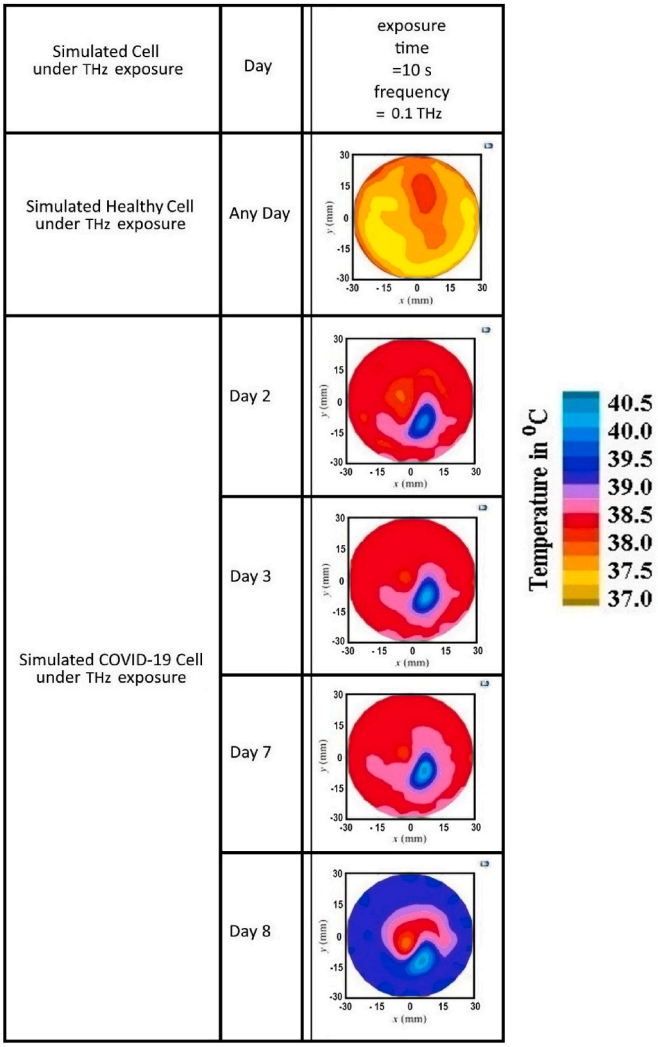

Fig. 8. Summary of THz thermographs (cross-sectional/planar view) of nCOVID-19 affected respiratory cell during the incubation period of virus infection: optimized exposure time = 10 s.

technique is beneficial for the early detection of coronavirus.

Terahertz imaging systems are good for non-ionizing radiation based detection of carcinoma. Also this can determine the tumour at early stage. However, terahertz radiation penetrating power through human body is a challenge. Most of the energy gets absorbed in water and thus researchers are trying hard to increase its penetrating power. Reduction of SNR by photon coupling technology can increase the penetration level but this has also certain limitations. The availability of suitable room temperature terahertz sources are also a big challenge as most of the sources are bulky and complex. Researchers are focusing in this direction to address the issue by developing a portable room temperature terahertz source that can be operated at room temperature. In addition to this, terahertz imaging application on human body is subject to ethical committee clearance and still now this is under trial.

3.1. AI-enabled THz thermograph analysis

The authors have customized an object detection algorithm, able to identify photographs and detect any abnormality in them. Some of the common performance metrics include confusion matrix, precision, recall (sensitivity) rate, specificity, and F- Score & last but not the least ROC and misclassification error curve [47–49]. The receiver operating characteristic (ROC) curve is a powerful tool for assessing and

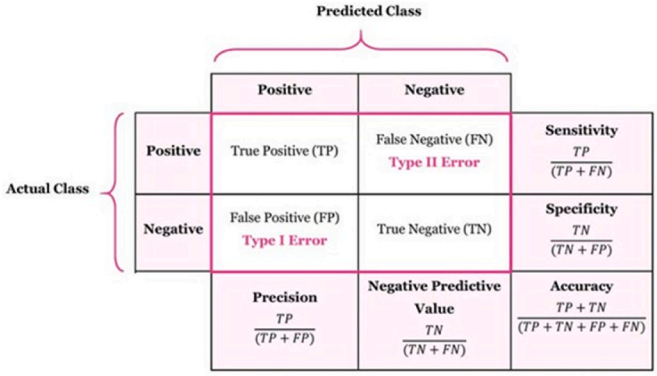

Fig. 9. Confusion matrix of the proposed AI model.

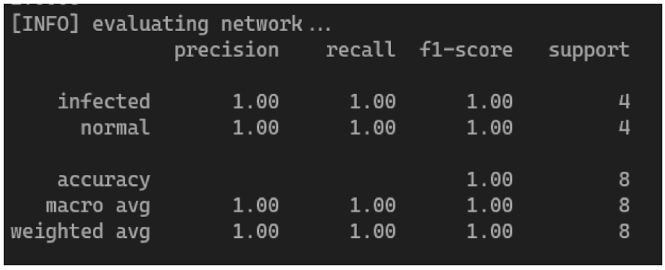

```
[INFO] evaluating network ...
              precision    recall  f1-score   support

    infected       1.00      1.00      1.00         4
      normal       1.00      1.00      1.00         4

    accuracy                           1.00         8
   macro avg       1.00      1.00      1.00         8
weighted avg       1.00      1.00      1.00         8
```

Fig. 10. Metrics for model accuracy evaluation.

contrasting different prediction models. ROC curves are a helpful tool for evaluating the accuracy of a prediction model's ability to separate genuine positives and negatives from false outcomes. The ROC curve does this by graphing sensitivity, the probability of correctly predicting a true positive, versus specificity, the probability of correctly predicting a true negative. Misclassification error is a measure in machine learning that indicates the proportion of data that were wrongly predicted by a classification model. Misclassification Error Rate can be defined as, number of inaccurate guesses divided by the number of total predictions. The misclassification rate value can range from 0 to 1. The lower the misclassification error, the more accurately a classification model can predict the response variable's consequences. The F-score or F-measure quantifies the accuracy of a binary class statistical assessment. It is derived from the precision and recall of the test, where precision is the number of true positive outcomes divided by the total number of positive results, including those that were incorrectly identified, and recall is the number of true positive outcomes divided by the total number of samples that should have been recognised as positive. In diagnostic binary classification, precision is also referred to as positive predictive value, while recall is also referred as sensitivity. The sensitivity score is indicative of the misclassification of positive cases. Hence higher the score lower is the positive misclassification rate. In other words, false-negative cases (Type II Error) are lower in number. As a rule of thumb, sensitivity should be high for any good model. Similarly,

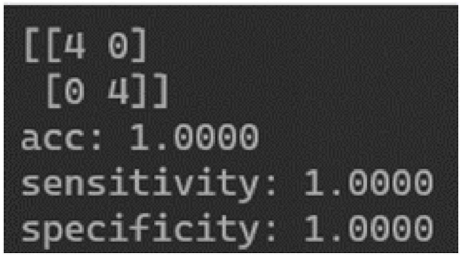

```
[[4 0]
 [0 4]]
acc: 1.0000
sensitivity: 1.0000
specificity: 1.0000
```

Fig. 11. Metrics of overall model accuracy evaluation.

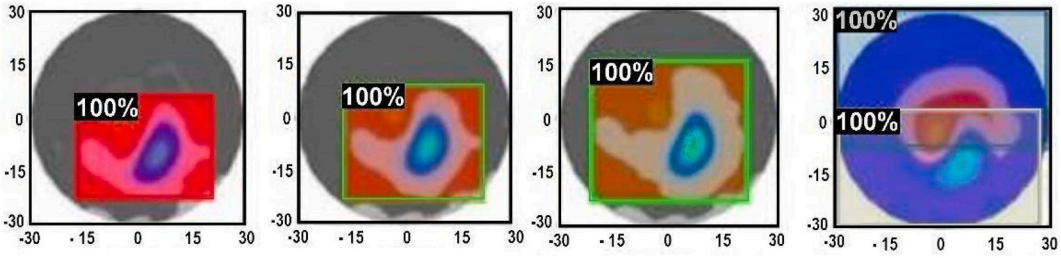

Fig. 12. Affected areas indicate COVID manifestation for different patients observed through AI model.

specificity is indicative of the misclassification of the negative cases. Hence higher the score lower is the negative misclassification rate. As explained earlier, a higher specificity indicates lower false-positive cases (Type I Error) in combination sensitivity and specificity contribute towards the overall accuracy. The same is illustrated in Fig. 9 and model evaluation on the test set is given in Fig. 10.

Going by the values shown in Fig. 11, the model performed 100% correctly on the 80 images in the test set. A detailed description of the confusion matrix is given in Figs. 10 and 11.

A test on smaller samples viz-a-viz 80 random test images may not be the right approach, so we passed all images to test the actual prediction. Out of 200 normal images, the ratio of correct to incorrect is 160:40 and out of 200 infected cases, the ratio of correct to incorrect is 200:0 which gives a total percentage of 90%. Hence the model is able to identify infected from the given dataset and further tests can be done to fine-tune the model and to increase the accuracy.

The power of explainable AI lies in the fact that the reason behind any classification can easily be known. The explanations are only used for the infected cases to demarcate the specific region in the scan as shown in Fig. 12. This segmentation gives a more comprehensive analysis of the amoebic pattern formation due to COVID infection. Fig. 12 shows the AI-assisted output images of the disease progression during days one to eight.

4. Conclusion

This paper reports a hybrid Covid 19/viral infection detection modality consisting of T-Ray as a radiation source for thermography method and AI-enabled tool for testing the efficacy of the modality. This is based on the difference of transmitted (after absorption in affected and non-affected cell/tissues) electromagnetic power/T-Ray power between healthy and virus affected cells that is reflected through temperature gradient study on thermographs. The variation of power absorption and associated temperature rise, in healthy and diseased cells, is due to the corresponding variation of electrical/dielectric/conductivity properties. THz thermograph technique is observed to be a potential non-ionizing technique in early diagnosis of Corona virus infected epithelium cells. The study for the first time reports the THz thermographs of COVID-19 infected epithelium cells and the spreading of the location of the affected zone with the advancement of infection days. This technique is found to be suitable for early detection of COVID infection at the cellular level and the findings may be correlated with the body's vital physiological parameters, including cardiovascular data, associated with Covid 19 to increase the efficacy of the screening technique. This is most useful for screening early Covid infection when conventional techniques cannot predict. Moreover, neighbouring cell damage issue due to THz radiation is insignificant. The validity of the model is established through AI tools. To the best of the authors' knowledge, this is the first report on early COVID-19 infection detection using AI guided Terahertz thermography.

Declaration of competing interest

The authors declare that they have no known competing financial interests or personal relationships that could have appeared to influence the work reported in this paper.

Acknowledgement

Moumita Mukherjee, the corresponding author, wishes to acknowledge (late) Prof. S K Roy and the research team at Defence R&D organisation, Government of India project, for providing laboratory support to do the experiment.

I would like to thank authors for the support of this research especially in covid times.

References

[1] Ritchie H, Mathieu E, Rodés-Guirao L, Appel C, Giattino C, Ortiz-Ospina E, et al. Coronavirus pandemic (COVID-19). Our world in data. 2020.
[2] Hou C, Chen J, Zhou Y, Hua L, Yuan J, He S, et al. The effectiveness of quarantine of Wuhan city against the Corona Virus Disease 2019 (COVID-19): a well-mixed SEIR model analysis. J Med Virol 2020;92(7):841–8.
[3] Kim D, Lee J-Y, Yang J-S, Kim JW, Kim VN, Chang H. The architecture of SARS-CoV-2 transcriptome. Cell 2020;181(4):914–21. e10.
[4] Ather Parvez Abdul Khalil Mr. Healthcare system through wireless body area networks (WBAN) using telosb motes. Int. J. New Pract. Manage. Eng. 2012;1 (02), 01 - 07. Retrieved from, http://ijnpme.org/index.php/IJNPME/article/view/4.
[5] Bazant MZ, Bush JW. A guideline to limit indoor airborne transmission of COVID-19. Proc Natl Acad Sci USA 2021;118(17):e2018995118.
[6] McCray Jr PB, Pewe L, Wohlford-Lenane C, Hickey M, Manzel L, Shi L, et al. Lethal infection of K18-hACE2 mice infected with severe acute respiratory syndrome coronavirus. J Virol 2007;81(2):813–21.
[7] Dimitrov DS. Virus entry: molecular mechanisms and biomedical applications. Nat Rev Microbiol 2004;2(2):109–22.
[8] Biswas S, Sen D, Bhatia D, Phukan P, Mukherjee M. Chest X-Ray image and pathological data based artificial intelligence enabled dual diagnostic method for multi-stage classification of COVID-19 patients. Aim Biophys 2021;8(4):346–71.
[9] Biswas S, Chakraborty C, Chawla R, Paul D, Sen D, Sarkar N, et al. A pragmatic approach for detecting nCOVID-19 using pervasive computing based on dual diagnostic measures. Int J Stat Med Res 2021;10:183–93.
[10] Biswas S, Sen D, Mukherjee M. PANDIT: an AI twin-based radiography image-assisted nCOVID-19 identification and isolation. Internet of things and its applications. Springer; 2022. p. 293–301.
[11] ProfBarry Wiling. Identification of mouth cancer laceration using machine learning approach. Int. J. New Pract. Manage. Eng. 2018;7. https://doi.org/10.17762/ijnpme.v7i03.66 (03), 01 - 07.
[12] Wong MD, Thai T, Li Y, Liu H. The role of chest computed tomography in the management of COVID-19: a review of results and recommendations. Exp Biol Med 2020;245(13):1096–103.
[13] Biswas S, Sen D, Bhatia D, Mukherjee M. COVED: a hardware accelerated soft computing enabled intelligent value Chain based diagnostic automation for nCOVID-19 estimation and identification. Int J Stat Med Res 2021;10:146–60.
[14] Rahul Sharma Mr. Modified golomb-rice algorithm for color image compression. 01 Int. J. New Pract. Manage. Eng. 2013;2:17–21. Retrieved from, http://ijnpme.org/index.php/IJNPME/article/view/13.
[15] Anish Dhabliya Mr. Ultra wide band pulse generation using advanced design system software. Int. J. New Pract. Manage. Eng. 2013;2 (02), 01 - 07. Retrieved from, http://ijnpme.org/index.php/IJNPME/article/view/14.
[16] Kaustubh Patil Mr. Optimization of classified satellite images using DWT and fuzzy logic. Int. J. New Pract. Manage. Eng. 2013;2 (02), 08 - 12. Retrieved from, http://ijnpme.org/index.php/IJNPME/article/view/15.
[17] Elena Rosemaro Ms. An experimental analysis of dependency on automation and management skills. Int. J. New Pract. Manage. Eng. 2014;3 (01), 01 - 06. Retrieved from, http://ijnpme.org/index.php/IJNPME/article/view/25.
[18] Antino Marelino Dr. Customer satisfaction analysis based on customer relationship management. Int. J. New Pract. Manage. Eng. 2014;3 (01), 07 - 12. Retrieved from, http://ijnpme.org/index.php/IJNPME/article/view/26.

[19] Sandip Kadam Dr. An experimental analysis on performance of content management tools in an organization. Int. J. New Pract. Manage. Eng. 2014;3 (02), 01 - 07. Retrieved from, http://ijnpme.org/index.php/IJNPME/article/view/27.
[20] Nora Zilam Runera Ms. Performance analysis on knowledge management system on project management. Int. J. New Pract. Manage. Eng. 2014;3 (02), 08 - 13. Retrieved from, http://ijnpme.org/index.php/IJNPME/article/view/28.
[21] Almeida MBd, Schiavo L, Esmanhoto E, Lenz CA, Rocha J, Loureiro M, et al. Terahertz spectroscopy applied to diagnostics in public health: a reviewvol. 64. Brazilian Archives of Biology and Technology; 2021.
[22] Peng Y, Shi C, Wu X, Zhu Y, Zhuang S. Terahertz imaging and spectroscopy in cancer diagnostics: a technical review. BME Frontiers 2020:2020.
[23] Yang X, Zhao X, Yang K, Liu Y, Liu Y, Fu W, et al. Biomedical applications of terahertz spectroscopy and imaging. Trends Biotechnol 2016;34(10):810–24.
[24] Smolyanskaya O, Chernomyrdin N, Konovko A, Zaytsev K, Ozheredov I, Cherkasova O, et al. Terahertz biophotonics as a tool for studies of dielectric and spectral properties of biological tissues and liquids. Prog Quant Electron 2018;62:1–77.
[25] Yu C, Fan S, Sun Y, Pickwell-MacPherson E. The potential of terahertz imaging for cancer diagnosis: a review of investigations to date. Quant Imag Med Surg 2012;2(1):33.
[26] Kasban H, El-Bendary M, Salama D. A comparative study of medical imaging techniques. Int J Info Sci Intelligence Syst 2015;4(2):37–58.
[27] Zhang X. Terahertz wave imaging: horizons and hurdles. Phys Med Biol 2002;47(21):3667.
[28] Arnone DD, Ciesla CM, Corchia A, Egusa S, Pepper M, Chamberlain JM, et al. Applications of terahertz (THz) technology to medical imaging. Terahertz Spectroscopy and Applications II: SPIE; 1999. p. 209–19.
[29] Johnson CC, Guy AW. Nonionizing electromagnetic wave effects in biological materials and systems. Proc IEEE 1972;60(6):692–718.
[30] Alon R, Sportiello M, Kozlovski S, Kumar A, Reilly EC, Zarbock A, et al. Leukocyte trafficking to the lungs and beyond: lessons from influenza for COVID-19. Nat Rev Immunol 2021;21(1):49–64.
[31] Lo S-CB, Chan H-P, Lin J-S, Li H, Freedman MT, Mun SK. Artificial convolution neural network for medical image pattern recognition. Neural Network 1995;8(7–8):1201–14.
[32] Acharyya A. 1.0–10.0 THz radiation from graphene nanoribbon based avalanche transit time sources. Phys Status Solidi 2019;216(7):1800730.
[33] Xuan Y, Roetzel W. Bioheat equation of the human thermal system. Chem Eng Technol: Indust Chem Plant Equipement Process 1997;20(4):268–76.
[34] Mehrotra P, Chatterjee B, Sen S. EM-wave biosensors: a review of RF, microwave, mm-wave and optical sensing. Sensors 2019;19(5):1013.
[35] Sze SM. Semiconductor devices: physics and technology. John wiley & sons; 2008.
[36] Taylor ZD, Garritano J, Sung S, Bajwa N, Bennett DB, Nowroozi B, et al. THz and mm-wave sensing of corneal tissue water content: in vivo sensing and imaging results. IEEE Trans Terahertz Sci Tecnol 2015;5(2):184–96.
[37] Girshick R, Donahue J, Darrell T, Malik J. Region-based convolutional networks for accurate object detection and segmentation. IEEE Trans Pattern Anal Mach Intell 2015;38(1):142–58.
[38] Pham V, Pham C, Dang T. Road damage detection and classification with detectron2 and faster r-cnn. In: 2020 IEEE international conference on big data (big data). IEEE; 2020. p. 5592–601.
[39] Li B, Yan J, Wu W, Zhu Z, Hu X. High performance visual tracking with siamese region proposal network. Proceedings of the IEEE conference on computer vision and pattern recognition2018. p. 8971-8980.
[40] Dharneeshkar J, Aniruthan S, Karthika R, Parameswaran L. Deep Learning based Detection of potholes in Indian roads using YOLO. 2020 International conference on inventive computation technologies (ICICT). IEEE; 2020. p. 381–5.
[41] Chen Z, Ho P-H. Global-connected network with generalized ReLU activation. Pattern Recogn 2019;96:106961.
[42] Adhikari S, Jayanthu S, Mukherjee M. Design and analysis of novel room temperature T-Ray source for biomedical imaging: application in full body prosthetics. Computer Vision and Machine Intelligence in Medical Image Analysis. Springer; 2020. p. 137–48.
[43] Adhikari S, LaRocco J, Saha R, Mukherjee M. Design & analysis of a terahertz power source for a non-invasive, non-ionizing imaging of full body prosthetics: a novel technique. J Phys Comput 2019;2(1):9–16.
[44] Biswas S, Sen D, Mukherjee M. In-silico studies of alzheimer's disease affected brain using a novel terahertz thermography technique. Advances in medical physics and healthcare engineering. Springer; 2021. p. 311–8.
[45] Adhikari S, Chakraborty D, Kundu A, Mukherjee M. Exotic IMPATT oscillator for terahertz thermography: feasibility studies in hepatic tumor detection. IETE J Res 2021:1–15.
[46] Adhikari S, Bhatia D, Mukherjee M. Super-lattice GaN/AlxGa1-xN nanoscale MITATT oscillator as terahertz radiation source: novel application in breast cancer imaging. Sens Int 2020;1:100014.
[47] Tharwat A. Classification assessment methods. Appl Comput Infomatic 2020;17(1):168–92. https://doi.org/10.1016/j.aci.2018.08.003.
[48] Visa S, Ramsay B, Ralescu AL, Van Der Knaap E. Confusion matrix-based feature selection. MAICS 2011;710(1):120–7.
[49] Goutte C, Gaussier E. A probabilistic interpretation of precision, recall and F-score, with implication for evaluation. In: European conference on information retrieval. Springer; 2005. p. 345–59.